5th Canadian Conf. Earthquake Engineering / Ottawa / 1987 / 5ème Conf. Canadienne Génie Sismique

Drained volume changes and undrained pore pressure increase mechanism for fly ash under cyclic triaxial loading

Hong Hsia & Ting Hu
Chengdu University of Science and Technology, Sichuan, People's Republic of China

ABSTRACT: Drained and undrained cyclic triaxial tests on fly ash are carried out under isotropical consolidation condition. An empirical model for soil volume changes is proposed. It is proved that the model can well predict the results of drained tests. Then, a unified pore pressure model is formed by combining the rational aspects of the two models suggested by W.D.L. Finn and K. Ishihara. The new model is shown effective in predicting the generation and development of pore pressure process under cyclic triaxial loading.

1 INTRODUCTION

The model for liquefaction mechanism presented by G.R. Martin and W.D.L. Finn et al (1975) has shown that an important relationship exists between the undrained pore pressure increments and the potential volumetrical strain increments under cyclic loading. However, the property of successive yielding of granular materials and the influence of effective stress path are not taken into account in this model. On the other hand, in the model presented by K. Ishihara et al (1975), residual pore pressure increments were determined by the effective stress paths in static tests, but the relevant effects of residual pore pressure, potential volume change and dynamic effective stress path were not investigated. The present study is intended to combine the three dominant factors into a compatible relationship, and to get some fundamental understanding of the process of pore pressure increase under cyclic loading. It should be pointed out that all the studies and conclusions presented here are based on the experimental data on fly ash which is not as common a cohesionless granular material as sand, but is somewhat similar to silt.

2 TEST MATERIAL

Test material used is fly ash from Jiang-you Power Plant. Jiang-you fly ash has a grain size ranging from 0.006 to 0.8 *mm*, median grain size 0.45 *mm*, coefficient of uniformity $C_u = 5.5$, specific gravity $G_s = 1.975$, maximum void ratio 2.29, minimum void ratio 0.705, and static effective strength $C' = 0.0$, and $\phi' = 35.7^0$ with relative density 53.5%.

3 VOLUME CHANGES IN DRAINED CYCLIC TRIAXIAL TESTS

Drained cyclic triaxial tests are carried out on an electro-magnetically controlled cyclic triaxial apparatus. A specially designed volume pickup is used in order to monitor the dynamic volume changes of specimens.

Jiang-you fly ash with relative density from 50-58% is tested in drained isotropical consolidation condition under cyclic triaxial loading, with the ambient pressure $\sigma_{3C} = 0.5$, 1.0, 1.5, 2.0, and 3.0 kg/cm^2, respectively. The coefficient of pore pressure, $B = 0.97$–0.98. The dry density difference between every two samples under the same all-round pressure prior to applying cyclic loads is less than 0.01 kg/cm^3. A typical oscillogram record is illustrated in Fig. 1.

The relationship between the plastic volumetric strain increment (Δv) and the number of cycles (N), with approximately equal dynamic stress ratio but different all-round pressures is illustrated in Figs. 2 (a) and (b). The total amount of plastic volumetric strain versus the dynamic stress ratio for the numbers of cycles 3 and 20, respectively, is shown in Figs. 3 (a) and (b).

The above figures show that:

1. The largest plastic volumetric strain increment is caused in the first cycle in laboratory tests. The volumetric strain increments in subsequent cycles become gradually smaller.

2. Plastic volumetric strains are not significanyly affected by the confining pressure. They are cyclic stress ratio dependent.

In addition, in Fig. 2, the application of cyclic stress

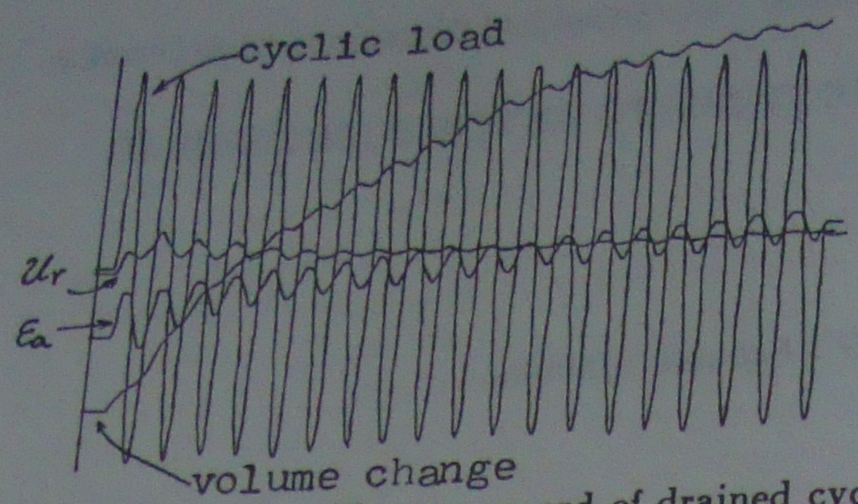

Fig. 1 A typical oscillogram record of drained cyclic triaxial tests.

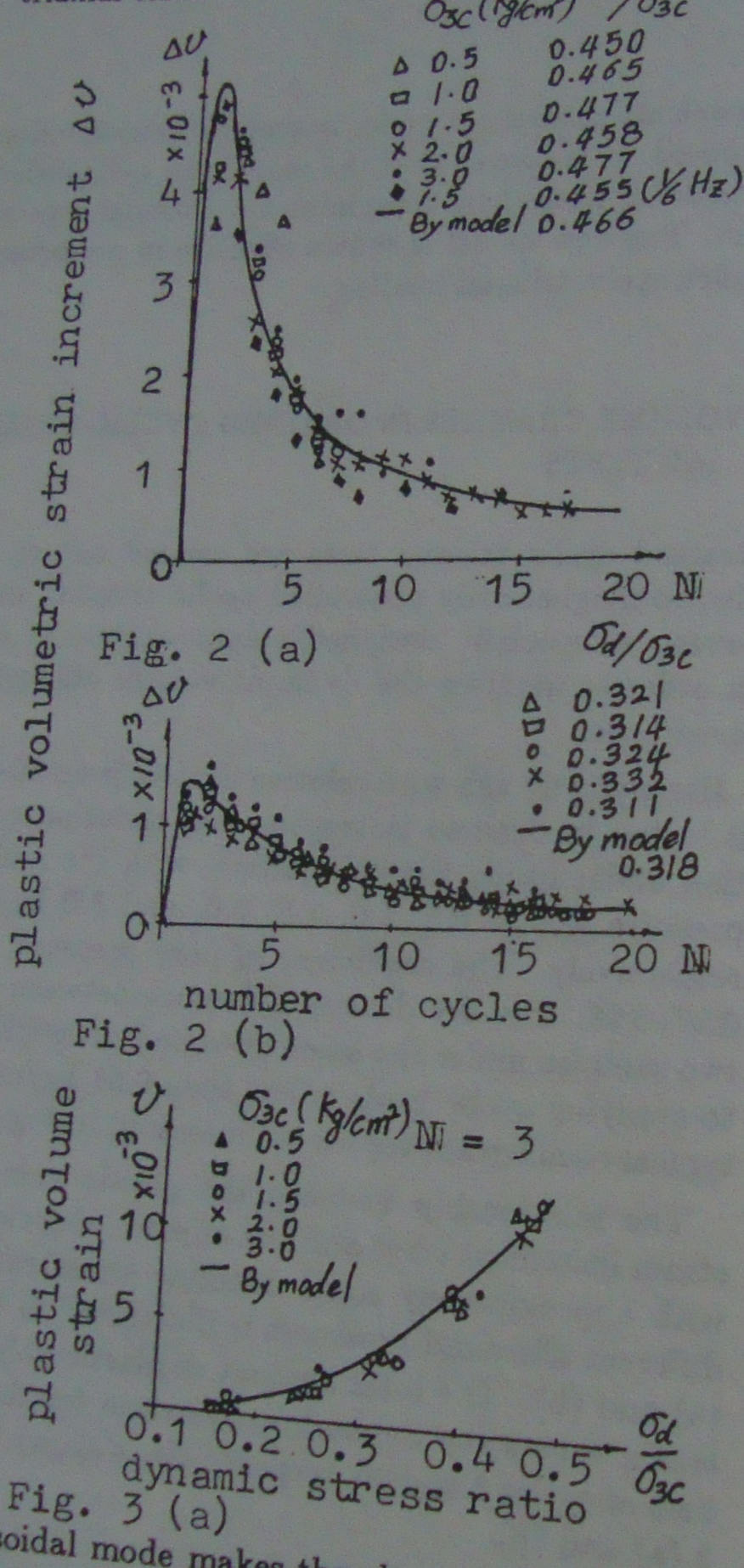

of sinusoidal mode makes the characteristics of volume changes in reloading process extremely obvious. This observation leads to point 3.

3. Plastic volume changes exist in any reloading process, eventhough the stress level during reloading may be equal to or less than the level during primary loading. The amount of the increment depends on the stress level in reloading and the number of cycles. In the analytical models used in the past, it has usually been assumed that a plastic volumetric

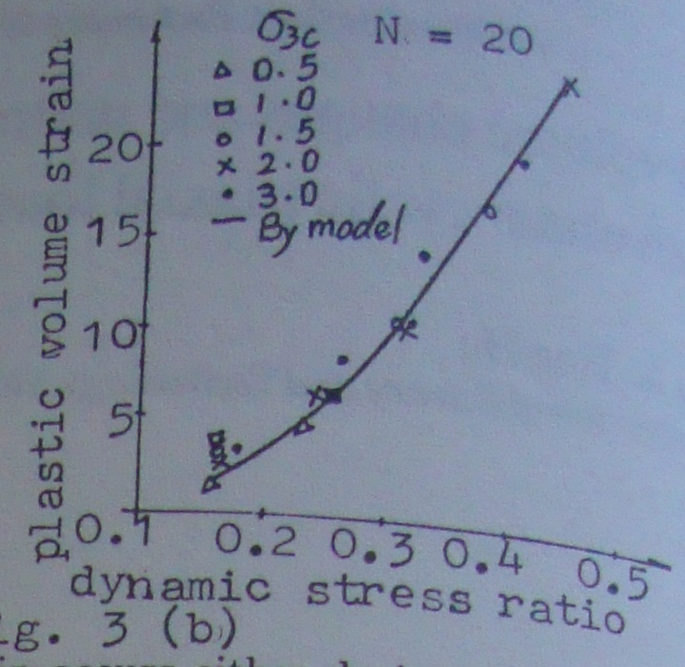

strain occurs either during primary loading or during reloading, in the latter case only when the stress level was large enough that the stress path crossed a previous yielding locus.

From Figs. 1 and 3, it is observed that the total amount of plastic volumetric strain keeps increasing either with the increase of number of cycles or with the increase of dynamic stress ratio. Such a phenomenon contradicts that exhibited by Jiang-you fly ash in static loading tests in which the volume swelling is prominent when the axial strain becomes large. It can therefore be stated that:

4. The dilatancy of Jiang-you fly ash under cyclic loading is much different from that under static monotonic loading.

According to the above investigation, the following postulates can be made in order to set up the concept of volume change model.

1. Plastic volumetric strains are dominated by dynamic stress ratio.

2. Plastic volumetric strain exists in either compression range or tension range, designated by Δv_C and Δv_T, respectively, and the two parts are independent of each other. Therefore, the total amount of plastic volumetric strain in a cycle is given by:

$$\Delta v_N = \Delta v_C + \Delta v_T$$

3. The characteristics of strains under cyclic loading can be better expressed by a nonlinear elasto-viscous-plastic model as shown in Fig. 4. The total amount of strain can be obtained from:

$$\{\epsilon\} = \{\epsilon_e\} + \{\epsilon_s\} \tag{1}$$

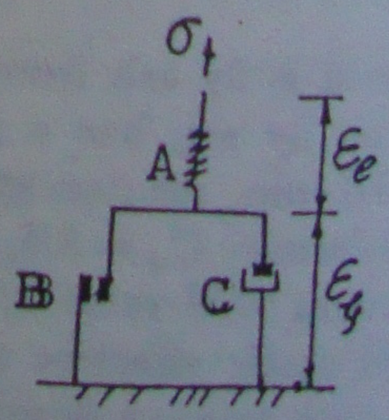

Fig. 4 Elasto-viscous plastic model.

4. The influence of frequency is not taken into account. A frequency change from 1/6 to 2 Hz produces little influence on the volume change (Youd, 1972).

Based on the above postulates, the increments of plastic volumetric strain in either compression or tension range versus the number of cycles are analysed and, with the help of experiments, an empirical volume change model for evaluating the increments of plastic volumetric strain is proposed:

$$\Delta v_N = \frac{K_2 N}{\sqrt{(1-N^2)^2 + K_1 N^2}} \tag{2}$$

Parameters K_1 and K_2 are related only to the stress conditions and can be expressed empirically as follows:

$$K_1 = \beta_1 e^{\frac{\beta_2}{R}} \tag{3}$$

$$K_2 = \alpha_1 \tan^{-1}\left[\frac{2\xi(\frac{R}{\alpha_2})}{1-(\frac{R}{\alpha_2})^2}\right] \tag{4}$$

and

$$K_2 \in (0, \alpha_1 \pi).$$

in which, $R = \sigma_d/\sigma_{3C}$ is dynamic stress ratio and β_1, $\bar{\beta}_2$, α_1, α_2 and ξ are model parameters depending on the properties of materials.

In the proposed model, the plastic volumetric strain increment depends only on the number of cycles and the dynamic stress ratio. Therefore, it is possible to determine all the parameters from test data of one set of specimens in cyclic drained triaxial tests with the same all-round pressure. The plastic volumetric strain increments in the first and the second cycle are read out from the oscillogram for each specimen with different dynamic stress ratio. Then the following relationship can be derived from Eq. (2):

$$\Delta v_1 = \frac{K_2}{\sqrt{K_1}}$$

$$\Delta v_2 = \frac{2K_2}{\sqrt{9+4K_1}} \tag{5}$$

Designating $\Delta v_1/\Delta v_2$ by ψ,

$$K_1 = \frac{9}{4(\psi^2-1)}$$

$$K_2 = \Delta v_1 \sqrt{K_1} \tag{6}$$

By substituting different values of Δv_1 and Δv_2 in Eq. (6), the values of K_1 and K_2 for different dynamic stress ratios can be calculated. Equation (3) is now rewritten as follows.

$$\bar{\beta}_2 = R \ln\left(\frac{K_1}{\beta_1}\right) \tag{3a}$$

Then K_1 is plotted as a function of R as shown in Fig. (5). When $R \to \infty$, $\beta_1 = K_{1min}$. From Eq. (3a) values of β_2, its mathematical expectation $\bar{\beta}_2$ and root mean square deviation σ_{β_2} can be obtained for different dynamic stress ratios. The value of β is now slightly increased or decreased and the same steps repeated until the minimum value of σ_{β_2} is reached. Then the values of β_1 and β_2 in the last step are taken as the model parameters.

To determine the other parameters, K_2 is plotted as a function of R as shown in Fig. 5(b). When $R \to \infty$, K_{2max} is obtained. From Eq. (4), we have

$$\alpha_1 = \frac{K_{2max}}{\pi} \tag{7}$$

Then, a value can be read off from the curve $K_2 \sim R$ corresponding to K_{2max}/π, and designated by R_m. Again, from Eq (4), we get

$$\alpha_2 = R_m \tag{8}$$

A value is chosen arbitrarily for ξ with $\xi \in (0,1)$. The curve represented by Eq. (4) is plotted next. The selected value of ξ is now increased or decreased till the curve coincides well with the experimental curve. This value of ξ is taken as the model parameter.

Figure 5 shows the curves of K_1 versus σ_d/σ_{3C} and K_2 versus σ_d/σ_{3C} for Jiang-you fly ash. The model parameters determined in accordance with the above method are as follows,

$\beta_1 = 0.3$, $\bar{\beta}_2 = 1.08$, $\alpha_1 = 5.73 \times 10^{-3}$, $\alpha_2 = 0.46$, $\xi = 0.35$.

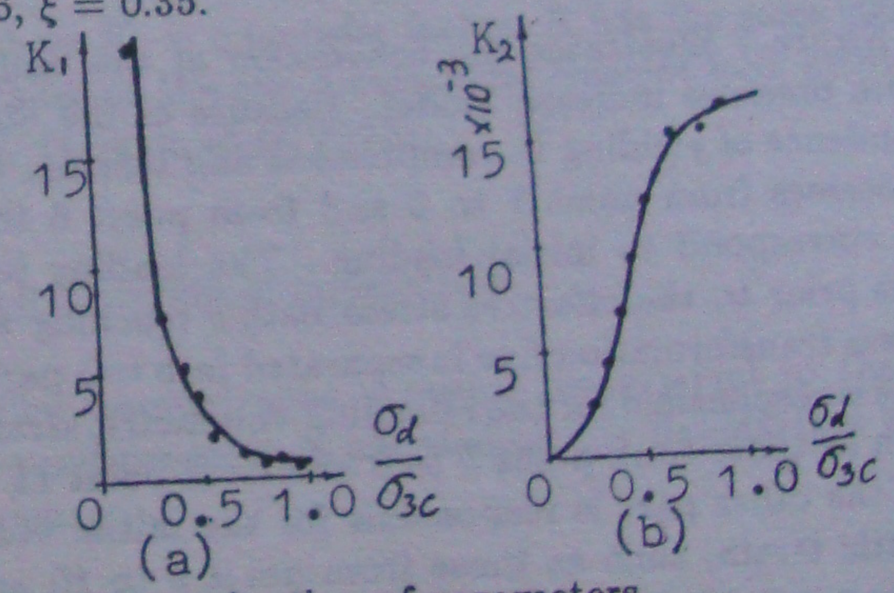

Fig. 5 Determination of parameters.

The relationships between plastic volumetric strain increment, Δv, and the number of cycles, N, for dynamic stress ratio, $\sigma_d/\sigma_{3C} = 0.466$ and 0.318 calculated on the basis of proposed model are illustrated in Figs. 2 (a) and (b), respectively. The predicted curves of v versus σ_d/σ_{3C} for $N = 3$ and 20 cycles are also illustrated in Figs. 3 (a) and (b). The agreement of all the predicted curves with the corresponding experimental data is very satisfactory.

Figure 6 shows the comparison between the calculated curve $v \sim N$ with $K_1 = 9.35$ and $K_2 = 4.38 \times 10^{-3}$ and the experimental data from a speci-

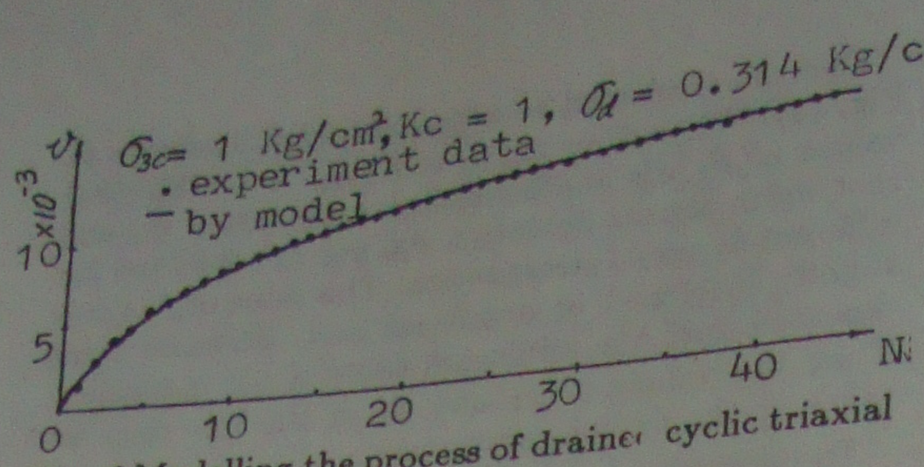

Fig. 6 Modelling the process of drained cyclic triaxial test.

men with $K_c = 1$, $\sigma_{3C} = 1.0\ \mathrm{kg/cm^2}$. The agreement is again very good.

4 PORE WATER PRESSURE INCREASE MODEL

In the authors' opinion, wherever there is the potential plastic volumetric strain caused in an undrained sample, a residual pore pressure increment must be built up to maintain the total volume of the sample unchanged. During liquefaction, the sample yields intermittently along the effective stress path and a corresponding potential plastic volumetric strain increment is caused. This increment can be changed into the equivalent amount of residual pore pressure by using the model by G.R. Martin and W.D.L. Finn (1975). In the next cycle, the sample is reloaded and yields again along the effective stress path from the stress state set up at the end of the previous cycle, accompanied by the build up of an additional plastic volumetric strain increment. Of course, in the process, additional residual pore pressure is certainly produced. This process continues till the sample is liquefied.

Figure 7 illustrates the convention of the unified pore pressure increase model. Because of the independence of yielding in compression and tension, the processes from point 1 to 2 and from point 6 to 7 all correspond to initial loading. The loading process prior to the effective stress path's reaching the phase transformation line is separated into two parts. One is responsible for the reloading volumetric strain, such as those from point 8 to 9 and from point 11 to 12; the other part is responsible for the initial volumetric strain, such as those from point 9 to 10 and from point 12 to 13. Plastic volumetric strains are also caused in the unloading processes after the effective stress path meets with the phase transformation line, such as those from point 18 to 19 to 20 and from point 22 to 23 to 24. During all the above processes, a certain amount of residual pore pressure is synchronously developed along with a potential plastic volumetric strain increment.

For uniform symmetric cyclic loading, the following postulates are made to form a unified pore pressure increase model.

4.1 Yielding loci

Yielding loci for cohesionless fly ash are assumed to

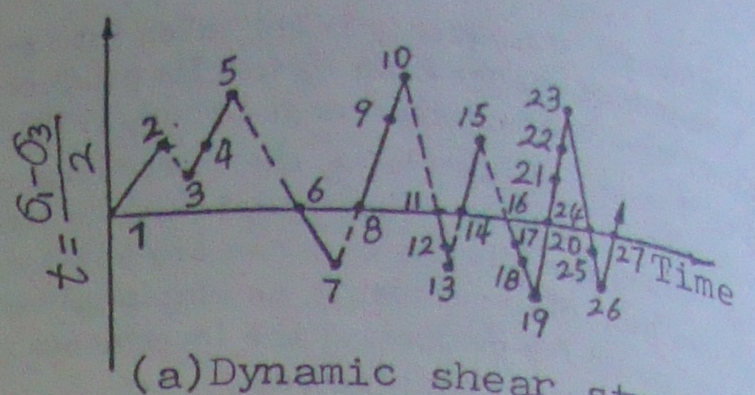

(a) Dynamic shear stress

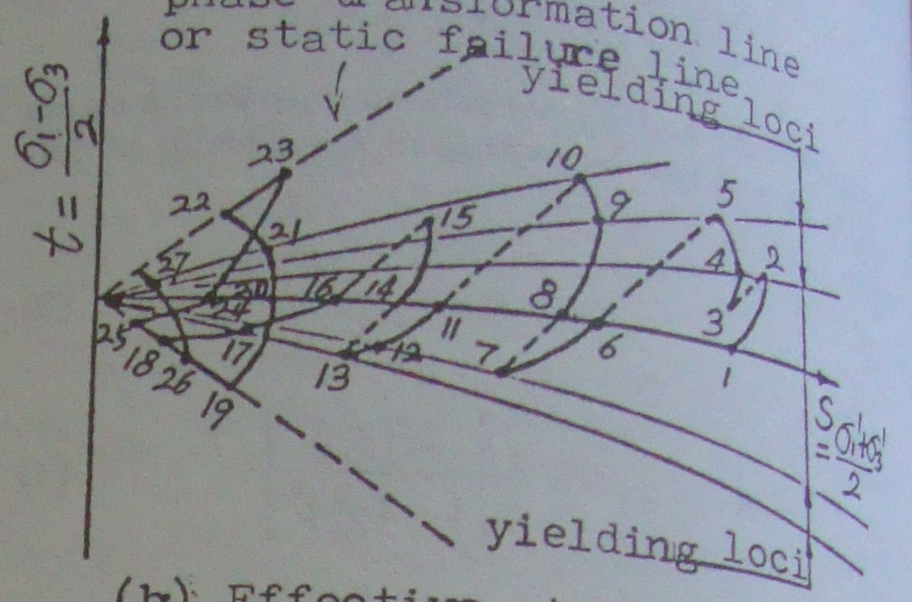

(b) Effective stress path

Fig. 7 Conception of the unified pore pressure increase model.

be straight lines originating from the origin of the coordinates, (t, s) as shown in Fig. 7. The equation can be expressed by:

$$t = K_{pi}\, s \tag{9}$$

where, K_{pi} is the slope of the yielding locus which is set up at the end of the i^{th} half cycle. Also,

$$K_{pi} = \frac{\pm\sigma_d}{2S_i \pm \sigma_d}$$

where, S_i is the effective confining pressure at the end of the i^{th} half cycle. a + sign is taken when in compression, and a – sign when in tension.

The maximum or minimum value of K_{pi} equals the slope of the phase transformation line in compression or tension, respectively $(\pm K_{p1})$. For loose or medium density, we can take $K_{p1} = \sin\phi'$, where ϕ' is the static effective internal friction angle of the material.

4.2 The reloading dynamic stress ratic and the initial dynamic stress ratio

For uniform cyclic loading, the current yielding locus that the effective stress path is to surpass in the i^{th} half cycle (in compression or in tension) is the locus set up at the end of the $(i-2)^{th}$ half cycle that separates the dynamic shear stress of the i^{th} half cycle into two parts, $\Delta\tau'_{Ri}$ and $\Delta\tau'_{Ii}$. Because

the pore pressure increment caused by reloading dynamic shear stress is much smaller, $\Delta\tau'_{Ri}$ and $\Delta\tau'_{Ii}$ can be replaced by $\Delta\tau_{Ri}$ and $\Delta\tau_{Ii}$, especively as

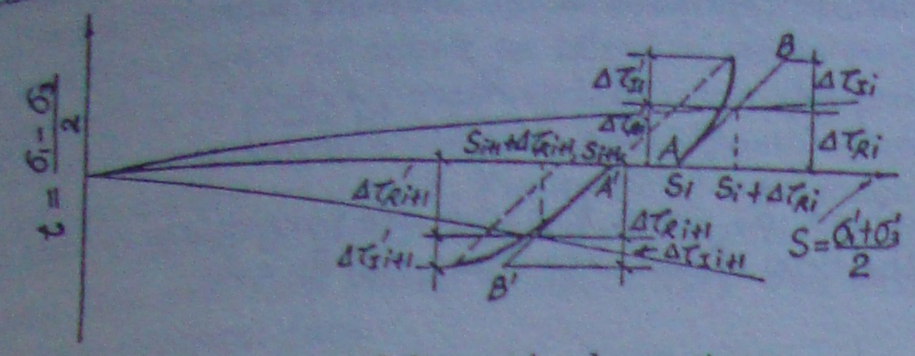

Fig. 8 Determination of dynamic shear stress.

shown in Fig. 8, in which the straight line AB represents the drained stress path with the angle of slope, 45^0. Therefore, for the i^{th} half cycle,

$$\Delta\tau_{Ri} = K_{p_{i-2}} \frac{S_i}{1 - K_{p_{i-2}}} \tag{10}$$

$$\Delta\tau_{Ii} = \pm\frac{\sigma_d}{2} - \Delta\tau_{Ri} \tag{11}$$

In the above, for $(i-2) \leq 0$, $K_{p_{i-2}} = 0$; and for $\mid K_{p_{i-2}} \mid \geq K_{p_1}$, $K_{p_{i-2}} = \pm K_{p_1}$; $\Delta\tau_{Ri}$ and $\Delta\tau_{Ii}$ are the reloading dynamic shear stress and the initial dynamic shear stress, respectively. Therefore, the dynamic stress ratios are given in the following forms,

For reloading:

$$R_{ri} = \frac{2\Delta\tau_{Ri}}{S_i} = \frac{2K_{p_{i-2}}}{1 - K_{p_{i-2}}} \tag{12}$$

For initial loading:

$$R_{Ii} = \frac{2\Delta\tau_{Ii}}{S_i + \Delta\tau_{Ri}} = \frac{\pm\sigma_d - 2\Delta\tau_{Ri}}{S_i + \Delta\tau_{Ri}} \tag{13}$$

4.3 Dynamic shear stress in the unloading processes

For the unloading processes in which the effective stress path has exceeded the path tranformation line, $\mid K_{p_{i-2}} \mid \geq K_{p_1}$. The dynamic shear stress in a half cycle is, in this case, separated into two parts. One is the reloading shear stress, $\Delta\tau_{Ri}$. The other part represents the dynamic shear stress which causes both the initial volume change and the plastic volume change in the unloading process, designated by $\Delta\tau_{Ii}$. These two parts of the dynamic shear stress are also obtained approximately from Eqs. (10) and (11); and R_{ri} takes the same value as given by Eq. (12); but R_{Ii} is expressed by:

$$R_{Ii} = \frac{2\Delta\tau_{Ii}}{S_f} \tag{14}$$

$$S_f = \frac{\sigma_d}{2K_{p_1}}$$

where S_f is the effective confining pressure at the point at which the unloading process starts.

4.4 Increments of plastic volumetric strain

The plastic volumetric strain increment, Δv_i, for any half cycle consists of two parts,

$$\Delta v_i = \Delta v_{Ri} + \Delta v_{Ii} \tag{15}$$

where, Δv_{Ri} and Δv_{Ii} are the reloading volumetric strain increment and the initial volumetric strain increment, respectively, for the i^{th} half cycle. They are calculated from Eq. (2) by substituting the appropriate number of cycles and the corresponding dynamic stress ratio from Eq. (12) or Eq. (13). When $\mid K_{p_{i-2}} \mid \geq K_{p_1}$, Δv_{Ii} represents the plastic volumetric strain increment during the unloading process for the i^{th} half cycle. It is obtained by substituting the value of N, which is the number of times that the effective stress path intersects the same phase transformation line in compression or in tension, and the dynamic stress ratio obtained from Eq. (14) into Eq (2).

4.5 Increment of pore water pressure

The increment of residual pore pressure in the i^{th} half cycle can be expressed by,

$$\Delta u_i = \bar{K}_r \Delta v_i \tag{16}$$

where $\bar{K}_r$ is a transfer factor. It has the same significance as the one-dimensional resilient bulk modulus $\bar{E}_r$ (Martin et al, 1975).

4.6 Criterion of liquefaction

The residual pore pressure being equal to the all-round pressure is adopted as the liquefaction criterion.

4.7 Elastic pore pressure increment

The elastic pore pressure increment in a cycle is considered to have little influence on the process of residual pore pressure increase and is neglected in this model.

Undrained cyclic triaxial tests are carried out for Jiang-you fly ash samples of medium density D_r = 50–55% with the application of uniform periodical sinusoidal loads and the all-round pressures σ_{3C} = 0.5, 1.0, 1.5, 2.0, 3.0 kg/cm^2, respectively, in isotropical consolidation conditions. The frequency used is

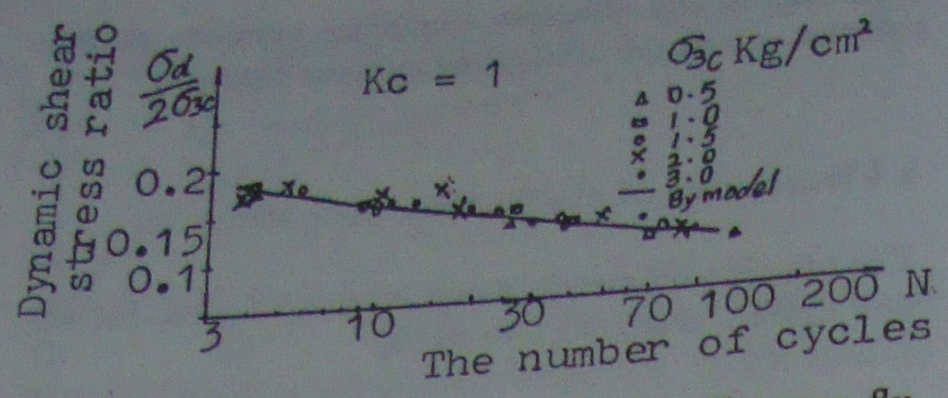

Fig. 9 Liquefaction resistance curve for Jing-you fly ash.

1 Hz. According to the initial liquefaction criterion, the dynamic shear stress ratios which cause the sample to liquefy is plotted against the number of cycles in Fig. 9. It is shown that the influence of all-round pressure on the relationship is not significant for this type of fly ash. Therefore, the transfer factor, $\bar{K}_r$ in Eq (16) can be normalized by the all-round pressure. Thus, $\bar{K}_r$ can be determined from only one set of tests with the same all-round pressure. This procedure is illustrated below by the set of tests of Jiang-you fly ash with the all-round pressure $\sigma_{3C} = 0.5$ kg/cm^2. The residual pore pressure increment in each cycle, ΔU_N, is calculated first for different dynamic stress ratios. The pore water pressure increment in the i^{th} half cycle in Eq. (26) can be approximately expressed as follows.

When i is odd,

$$\Delta u_i = \frac{\Delta v_{i-2}}{\Delta v_{i-1} + \Delta v_{i-2}} \Delta U_N \qquad (17a)$$

$$\Delta u_{i+1} = \Delta U_N - \Delta u_i \qquad (17b)$$

When $(i-2) \leq 0$, $\Delta u_1 = \frac{1}{2}\Delta U_1$, and $\Delta u_2 = \frac{1}{2}\Delta U_1$ and N takes the integer value of $i/2$.

When all the values of Δu_i are obtained from a set of tests, the proposed pore pressure increase model can be used to determine the potential volumetric strain increment of every cycle, Δv_N. Then, the ratio $\Delta U_N/\Delta v_N$ can be obtained to represent the transfer factor $\bar{K}_r$. Finally, the relationship between $\bar{K}_r/\sigma_{3C}$ and the total residual pore pressure ratio, u/σ_{3C} can be evaluated.

Figure 10 shows the relationship obtained as above for Jiang-you fly ash with the all-round pressure σ_{3C}

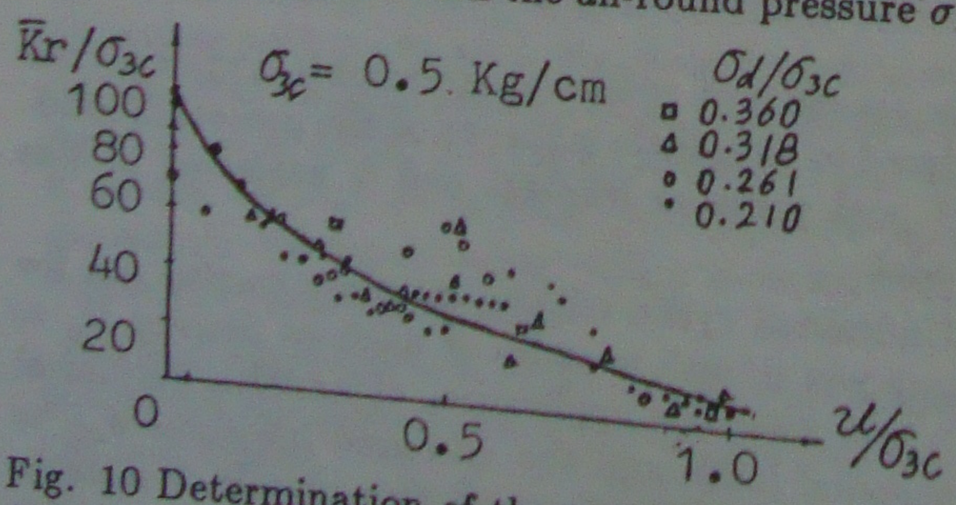

Fig. 10 Determination of the transfer factor in unified pore pressure model.

$= 0.5$ kg/cm^2. The scattering of data in the figure is considered to be due to the original recording and the simplified calculation. None the less, the relationship can be expressed in the following form:

$$\frac{\bar{K}_r}{\sigma_{3C}} = \frac{\bar{K}_{r0}}{\sigma_{3C}} - b\left(\frac{u}{\sigma_{3C}}\right)^r \qquad (18)$$

where, $\bar{K}_{r0}/\sigma_{3C}$, b, and n are parameters related to the type of soil. For Jiang-you fly ash:

$$\frac{\bar{K}_{r0}}{\sigma_{3C}} = 100,\ b = 94,\ n = 0.5$$

The liquefaction resistance curve obtained from the proposed model for Jiang-you fly ash is shown in

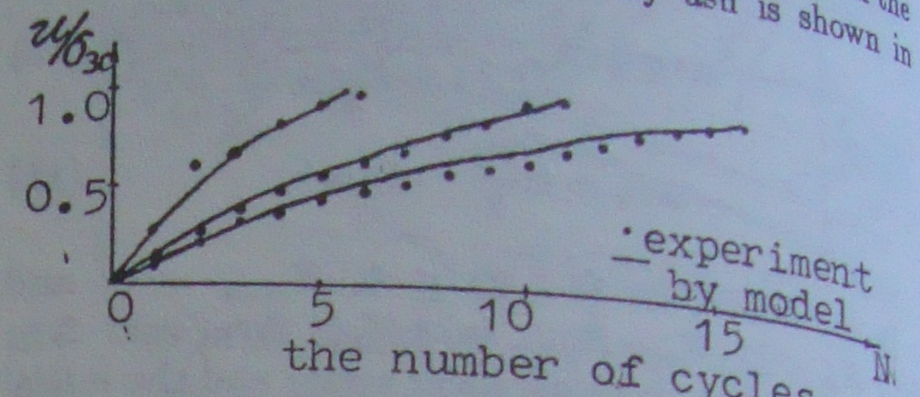

Fig. 11 Prediction of the pore pressure increase for Jiang-you fly ash.

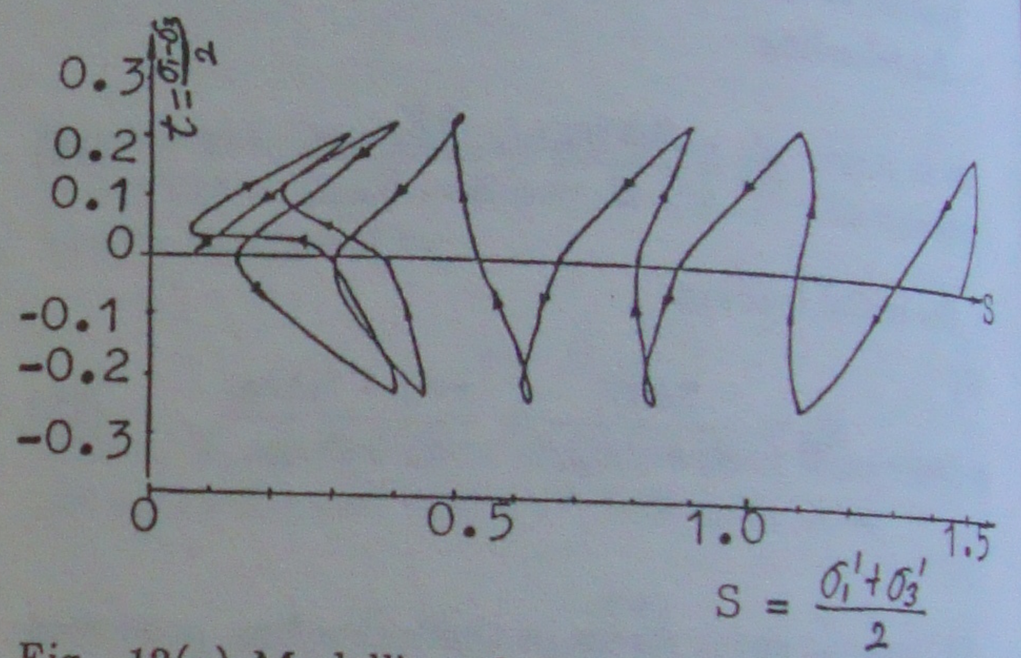

Fig. 12(a) Modelling the process of effective stress path for Jiang-you fly ash.

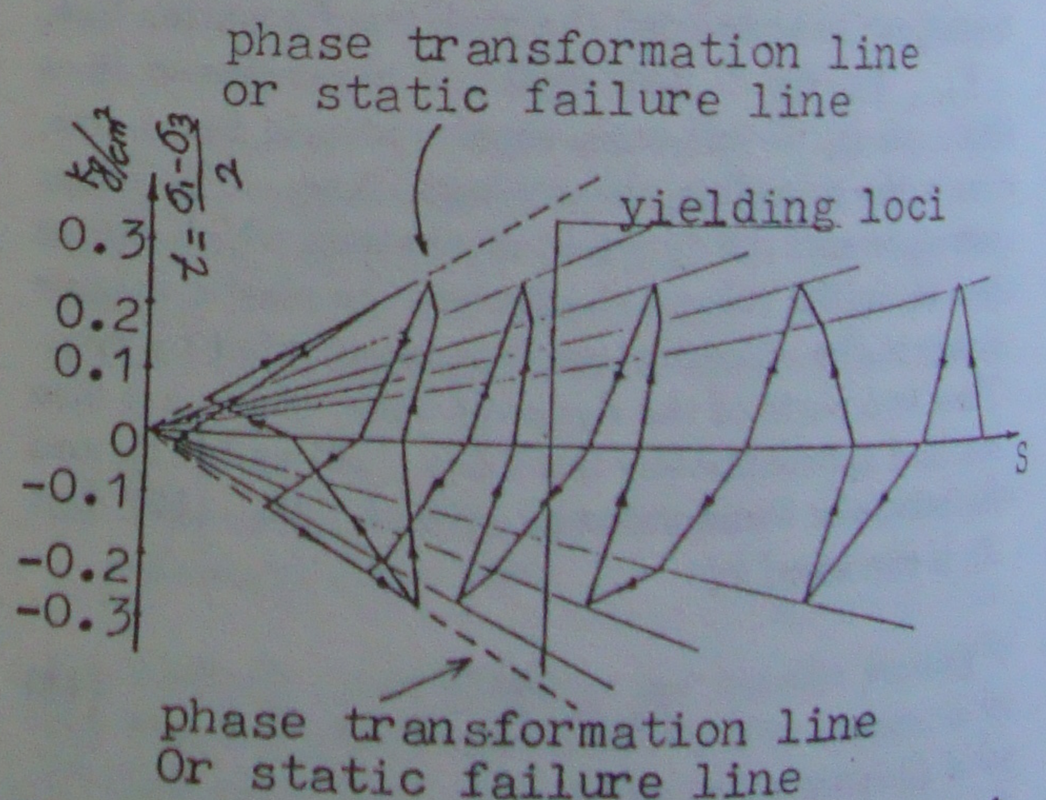

Fig. 12(b) The experimental effective stress path of a sample of Jiang-you fly ash

Fig. 9 by a solid line. Figure 11 shows the residual pore pressure increase against the number of cycles again obtained from the proposed model. Also shown is the same relationship obtained from an experiment. Figure 12 shows an effective stress path obtained from the proposed model during the process of liquefaction, in which the elastic dynamic pore pressure is taken as $\pm\sigma_d/3$. Figure 12(b) is an example of an actual sample's effective stress path. In all cases, the predicted values compare very well with the experimental data.

From the study reported in this paper, some important conclusions can be drawn. They are summarized below.

5 SUMMARY AND CONCLUSIONS

Drained and undrained cyclic triaxial tests on fly ash are carried out under isotropical consolidation conditions. By analysing the drained test data, the following characteristics of volume changes under cyclic triaxial loading are obtained:

1. For cohesionless granular materials such as fly ash, the plastic volumetric strain increment is definitely caused during any reloading process with the application of cyclic loading, even though the drained effective stress path does not surpass any new yielding locus of the material during this process.

2. In cyclic loading tests of reversing direction, the dilatancy phenomenon is much different from that in static monotonic loading.

An empirical model for evaluating the plastic volumetric strain increments for cohesionless fly ash is proposed, which can be used for uniform cyclic loading in isotropical consolidation conditions. The comparison between the experimental data and the predicted values proves the effectiveness of the model.

Further, through an analysis of cyclic undrained tests on saturated specimens of fly ash and with the help of the study of the volume changes, a unified pore pressure increase model is suggested. The model combines the rational aspects of the two models proposed respectively by G.R. Martin, W.D.L. Finn et al, and by K. Ishihara et al. It is shown that the processes and the onset of liquefaction for fly ash under isotropical consolidation conditions with the application of uniform cyclic loading can be well predicted by the suggested unified pore pressure increase model, which possesses the following characteristics:

1. The relationship among the residual pore pressure increment, the potential volume change, and the effective stress path is considered in this model.

2. Even if the undrained effective stress path does not go across the previous yield loci during any reloading process, an increment of residual pore pressure is still caused.

3. The fact that the residual pore pressure increments are also generated during the unloading processes after the effective stress path has reached the phase transformation line and thereafter turns its direction is taken into account empirically.

The present study attempts to illustrate another method of investigating the complicated process of liquefaction. Much more sophisticated and detailed work is needed to make the ideas in this paper more reliable and practical.

6 REFERENCES

Castro, G. 1975. Liquefaction and cyclic mobility of saturated sands. Jour. of the Geotech. Eng. Div. ASCE. Vol. 101, No. GT6.

Hu, Ting 1981. The shear modulus and deformation of soils under cyclic loading. Proc. of the international conference on recent advances in Geotechnical Earthquake Engineering and Soil Dynamics, Vol. 1. St. Louis, U.S.A.

Ishihara, K., F. Tatsuoka, and S. Yasuda 1975. Undrained deformation and liquefaction of sand under cyclic stress. Soils and Foundations, Vol. 15, No. 1, March.

Martin, G.R., W.D.L. Finn, and H B. Seed 1975. Fundamentals of liquefaction under cyclic loading. Jour. of the Geotech. Eng. Div. ASCE Vol. 105, No. GT5.

Tatsuoka, F. and K. Ishihara 1974. Drained deformation of sand under cyclic stress reversing direction. Soils and Foundations, Vol. 14, No. 3, September.

Youd, T.L. 1970. Densification and shear of sand during vibration. Jour. of the Soil Mechanics and Foundation Engineering Division, ASCE. Vol. 96, No. SM3, May.

Youd, T.L. 1972. Compaction of sands by repeated shear straining. Jour. of the Soil Mechanics and Foundation Division, ASCE. Vol. 98, No. SM7, July.